Citation: Zhaoyang Cui, Xiaoli Zhao, Weikun Jia, et al. Effect of sodium chloride on enhanced performance of chitosan-based ion actuator. *Journal of Harbin Institute of Technology (New Series)*. DOI:10.11916/j.issn.1005-9113.2023119.

Effect of Sodium Chloride on Enhanced Performance of Chitosan-Based Ion Actuator

Zhaoyang Cui[1], Xiaoli Zhao[2], Weikun Jia[2], Yueming Ren[1], Yan Xu[2] and Yanzhuo Lv[1*]*

(*1. College of Material Science and Chemical Engineering, Harbin Engineering University, Harbin 150001, China;*
2. College of Mechanical and Electrical Engineering, Harbin Engineering University, Harbin 150001, China)

Abstract: In this work, an actuate membrane and an electrode membrane were prepared by a sol-gel method. And then, they were physically pressed to form a chitosan-based ion actuator (CSIA). Importantly, the effect of sodium chloride on CSIA were investigated, the mechanical properties of CSIA were tested by establishing an output force test platform and a displacement test platform while testing its porosity. And, the electrochemical performance was tested by electrochemical workstation. At the end, the surface morphology and functional groups were measured by scanning electron microscopy and Infrared spectrogram, respectively. The results indicated that the molar concentration of the sodium chloride was the best at 0.06836 mol · L^{-1} for CSIA. Its mechanical properties could reach an output force of 2.939 mN and a deflection displacement of 4.025 mm, and the maximum porosity of 12.98 % at the same time. The specific capacitance of the electrochemical performance was up to 0.07719 F · g^{-1}, and the minimum resistance reached 13.48 Ω. From the surface morphology and functional groups, the appropriate doping ratio of NaCl into CSIA was helpful for increasing the transport space of internal ions. The effective internal ion concentration and significantly reduced internal stress provided excellent performances under the appropriate voltage conditions. The doping of inorganic ion sodium chloride improved the internal electron transport efficiency of chitosan ion actuator, and it advanced the mechanical properties of the actuator. Hence the enhancement of NaCl output force in CSIA had a good significance for the development of inorganic salt ion strengthened ion actuator.

Keywords: sodium chloride; chitosan; doped; ion actuator

CLC number: O636 **Document code**: A **Article ID**: 1005-9113(2024)00-0000-13

0 Introduction

In the process of productivity development and technological innovation, traditional mechanical methods can no longer meet the current development trend of miniaturization, portability, intelligence and precision on account of their low efficiency and high energy consumption[1-4]. Because of the advantages of light weight, low manufacturing cost, low actuating voltage, good flexibility and fast response speed, ion actuator had extremely important application potential in aerospace, underwater equipment, biomedicine, micro-robotics and other fields[5-7]. In recent years, the researchers found that the actuate membrane materials including sodium alginate[8], cellulose, chitosan[9-12]. Due to their unique three-dimensional network structure and ability to retain a large amount of water, ion actuator had a wide range of applications in hydrogel artificial muscles[13] including biomedical applications, drug carriers[14-15], biosensors[16], medical devices[17], tissue engineering[18], separation systems[19-20], microfluidic systems[21], microvalves[22] and actuator[23-24]. Chitosan (CS) was a product of natural chitin. Owing to its rich hydroxyl and amino groups, the chemical properties of CS were more active. This was able to improve its strength, heat resistance, elastic modulus, electrical conductivity and other abilities through a variety of chemical modification reactions, while having good biocompatibility and biodegradable characteristics[25].

According to the conductive mechanism, ion actuator was divided into inorganic salt ion conductive actuator and ionic liquid conductive actuator. The preparation methods of ion actuator were generally

Received 2023-10-26.

* Corresponding author. Yan Xu, Ph.D, Senior Experimentalist. Email: xychangke@163.com.
Yanzhuo Lv, Ph.D, Associate Professor. Email: Lvyanzhuo@hrbeu.edu.cn.

classified into two types. One of them was to put inorganic salts into an ionic solution formed by the formed hydrogel material, after that the ions penetrated into the hydrogel network to obtain ion actuator. And the other one was to use the one-pot method, which it added all raw materials including inorganic salt ions into the reaction system to form an ionic conductive hydrogel. Compared with traditional doping reagents, NaCl had the more reliable purity and raw material price advantages, and the process flow was relatively simple without complex side reaction impurities. However, ion actuator still had the problems of small mechanical properties and narrow doping improvement paths. At the meantime, the preparation of chitosan-based ion actuator (CSIA) by NaCl dissolved in gel solution had not been tested, and the effect of CSIA materials on the output performance and electrochemical performance of gel material actuator needed to be further studied.

Therefore, this work proposes to immerse ionic conductive hydrogels in inorganic salt ion solutions by physical doping process to just the proportion of inorganic salt Na^+ ions. Then, the effect of sodium chloride on CSIA was studied by testing the mechanical properties, porosity, electrochemical properties, and surface morphology and functional group measurements.

1 Experiments

1.1 Experimental and Reagent

Force measurement software (FA1004) was produced by Shanghai Shangping Instrument Co., Ltd (Shanghai, China). Vacuum drying oven (DZF-6050) was produced by Shanghai Sead Instrument Co., Ltd (Shanghai, China). Electrochemical workstation (CHI760E) was produced by Shanghai Chenhua Instrument Co., Ltd. Infrared spectroscopy (FT-IR200) was produced by Tianjin Gangdong Technology Development Co., Ltd. Scanning electron microscope (S-240) was produced by Cambridge Instrument Company. Digital micrometer produced by Guilin Haoli Measuring Instrument Technology Co., Ltd. Analytical balance (JJ224BC) produced by Changshu Shuangjie Testing Instrument Factory.

Chitosan (CS), sodium chloride (NaCl), acetic acid (HAC), Multi-walled carbon nanotubes (MCNT), Glycerol were provided by Shanghai Aladdin Bio-Chem Technology Co., Ltd (Shanghai, China). All chemicals were of analytic grade and used without treating further for purification and the deionized water was self-restraint.

1.2 Preparation of Chitotan-Based Ion Actuator

Chitosan-based ion actuator was a new type of responsive electronic material, mainly composed of electrode membranes and actuate membranes.

Chitosan-based ionic actuator was a new type of responsive electronic material, which mainly consisted of electrode membranes and actuate membranes prepared by sol-gel method[26] and its detailed preparation was shown in Fig. S1 in Supporting Information. The detailed preparation of NaCl-doped CSIA in this experiment was shown in Table S1 in Supporting Information. The CSIA actuator had a length and width of 30 mm×3 mm and an average thickness of 0.4 mm. The MCNT electrode film thickness was 0.1 mm (micrometer measurement) and the electrode film mass percentage was 41%.

1.3 Experimental Setup

1.3.1 Output force and displacement test of CSIA

The force test platform was shown in Fig. S2(a) in Supporting Information, under the experimental test conditions of 300 s, voltage of 3 V and baud rate of 9600, the output force test of CSIA samples from S_0 - S_5 was carried out, and the output force experimental test data of 6 groups were averaged. The deflection of CSIA on electrical stimulation was shown in Fig.S2(b) in Supporting Information.

Since the ion channel could improve the transmission ratio of charged ions inside the actuate membrane of CSIA, its mechanochemical characteristics and the porosity of the actuate membrane[27]. The formula for calculating porosity was shown below.

$$P = \frac{m_1 - m_0}{\rho \times V} \times 100\% \quad (1)$$

where P is the porosity of the drive membrane. m_0(g) is the constant mass of the actuate membrane. m_1(g) is the mass weight. ρ(g·cm^{-3}) is the density of absolute ethanol and V(cm^3) is the volume of the samples, respectively.

1.3.2 Electrochemical testing of CSIA

The electrochemical tests were tested by the electrochemical workstation, as shown in Fig. S4(a). The three-electrode system (Fig. S4(b)) was formed by using saturated calomel electrode as reference electrode and platinum electrode as auxiliary electrode and working electrode. The CHI760E was used for

cyclic voltammetry (CV) test and electrochemical impedence spectroscopy (EIS) test. The volt-ampere characteristic was curve obtained by the actuate membranes at 20 $mV \cdot s^{-1}$, 50 $mV \cdot s^{-1}$, 100 $mV \cdot s^{-1}$ scanning speeds. Because the clamping part of the electrochemical analyzer and the actuate membrane might had certain poor contact and the voltage instability when the instrument started, so the method of cyclic scanning was used to obtain three sets of voltammetry characteristic curve data at scanning speed. Calculating the area enclosed by the plotted figure, which was approximately the value of the integral part, and then it was brought into the specific capacitance formula[28] to calculate the specific capacitance (C_p) of the material. The specific capacitance was calculated as follows.

$$C_p = \frac{A}{2(V_2 - V_1) \times m \times k} \tag{2}$$

where C_p was the specific capacitance. A was the scanning area. V_1 and V_2 were low and high potential, respectively. m was the sample quality and k was the scanning speed.

The equivalent circuit model was indicated in Fig. S4(c). It was used to study the electrochemical impedance data[29]. This analog circuit used R_s to represent the resistance of the electrolyte solution, R_{ct} to denote the charge transfer resistance, C_d to show the electric double-layer capacitance, and W_o to represent the open potential. Data fitting was performed using Z-view software. The reverse extension of the data in the figure was connected to the x-axis, and its intercept was the measured resistance value.

The electrochemical performance of a CSIA sample was measured by its conductivity, which was calculated as follows.

$$\sigma = \frac{L}{R_s \times S} \tag{3}$$

where σ represented conductivity ($S \cdot m^{-1}$), R_S was resistance(Ω), S was area(m^2), and L was length (m).

1.3.3 Morphology and functional group testing of CSIA

The surface morphology of $S_0 - S_5$ of the CSIA sample was microscopic by high-resolution scanning electron microscope (SEM). By Fourier transform, the infrared spectrum in the range of 4000-400 cm^{-1} was marked with potassium bromide (KBr) particles to study the chemical molecular structure and physical doping reaction of the actuate membrane.

2 Results and Discussion

2.1 Effect of NaCl on Mechanical Properties of CSIA

The output force and time curves of different CSIA samples were shown in Fig. 1(a), from which it could be concluded that from S_0 to S_4, with the increase of the doping ratio of NaCl, the maximum output force of the CSIA sample S_4 reached 2.939 mN, which was 3.4 times higher than that of the control group S_0. With the doping ratio continuously increased, the output force decreased to 0.3020 mN for S_5 sample, and it reached 54.72% of S_0. This showed at an appropriate amount NaCl doping, it had a certain optimization of the network structure of the actuate membranes of CSIA, this could improve the ion transfer rate inside the actuate membranes, thereby the output force of the CSIA was improved, but an excessive doping would change the arrangement frame of the internal structure of the actuate of CSIA, it weakened its performance, leading to serious deformation bubbling and energy loss in the sample during the electrical stimulation response.

As shown in Fig. 1(c), the CSIA sample S_5 increased the doping over S_4, and then the displacement offset maximum began to decrease by 76.7% of S_4, indicating that the doping ratio of NaCl began to excess.

The relationship between the maximum output force of the sample CSIA and the porosity of the actuate membranes were shown in Fig.1(b), the trend of the two sets of data were the similar, with the increase of NaCl doping ratios, the change trend of porosity and output force increased first, and the porosity of actuate membranes CSIA of NaCl-doped reached the maximum at S_4, and the maximum attained 12.98%, The lowest of porosity decreased at S_5. This showed that NaCl had a certain optimization of the internal three-dimensional network structure of CS, which could improve the ion transfer rate inside the actuate membranes of CSIA, but over NaCl cross-linking doping would lead to beyond ion blockage inside the actuate membranes, the water content of the actuate membranes would decrease, and the CSIA would lose water and harden, resulting in the greater internal stress during deflection, thereby it weakened the output force. The specific performance

parameters of CSIA were detailed in Table S2.

The displacement deflection versus time was shown in Fig. 1(c), from which it can be concluded that the largest displacement deflection of the samples was S_4, and the deflection change reaches its maximum when it reaches 4.025 mm around 700 s, and then finally stabilizes to 3.9 mm after 1000 s. The other samples were first subjected to a slow fluctuating rise and then leveled off after 1000 s. The other samples were first subjected to a slow fluctuating rise and then leveled off after 1000 s.

Among them, the curves of sample S_3 in Fig.1(a) and S_4 in Fig.1(c) increased first and then decreased, and the reason for the curve fluctuation was mainly the occurrence of tremor. Due to the dehydration of the CSIA sample after work, the toughness of the material decreased and became brittle, resulting in the dynamic equilibrium of the CSIA's mechanical properties being slowly broken and causing tremor.

In addition, the final deflection state diagrams of samples with different NaCl doping ratios at 5 V were shown in Fig.S3. The test point for testing the deflection differed from the deflection at the farthest end of the deflection, which was due to the fact that the infrared test point was chosen to measure the farthest end of the point that was 3 mm inward. The trend of both deflections is basically the same, reaching the maximum deflection at sample S_4, which coincides with the maximum output force trend above.

However, it was also found that the bending repeatability of the actuator was poor, probably because air bubbles appeared on the surface and inside the actuator at the end of the output force test and displacement test, which resulted in the almost loss of braking performance of the prototype, so the output force and displacement deflection performance of the CSIA prototypes and its reusability required improvement.

As can be seen from Fig.1(a, c), when the maximum value of output force and displacement deflection both appear in sample S_4, CSIA sample showed a trend of first increased and then decreased in S_0 to S_5. In general, there was a positive correlation between output force and displacement deflection.

Researchers[30] pointed out that the deflection mechanism of the ion actuator aceration mechanism of the cellulose backbone was that under the action of electric field, the charge was injected into the cathode and the anode to form an electric double layer. The positively charged cation $-NH_3^+$ was bound by the polymer CS backbone and was fixed with the action of Van der Waals force. The anion $-CH_3COO^-$ moved towards the anode side of the electrode, and accumulates with increasing concentration over time, while the cation moved in the direction of the cathode. Based on above, the cathodic deflection of the actuator on a weakly acidic solution biogel was used, and this cathodic deflection phenomenon was mainly the result of internal ion movement.

As shown in Fig. 1(d), the CS molecule contained a large amount $-NH_2$, in the aqueous acetic acid solution, the backbone chain hydrolysis of CS, many free amino groups on the internal ions bind H^+ in the solution, so that chitosan became $-NH_3^+$ polyelectrolyte, while the remaining anions were in a free state to dissolve $-CH_3COO^-$ of CS. As shown in Fig. 1(e), in the CSIA actuate membranes after NaCl doping, Na^+ ions were concentrated near the cathode electrode membrane, because the ion radius of Na^+ ions (0.97Å) was less than $-CH_3COO^-$ ion radius (4.50 Å), so when the concentration on both sides accumulated to a certain amount, the ion concentration difference on both sides was inside the actuate membranes under the action of Van der Waals force to make the surface of the electrode showing stress and bending strain. Since the ionic radius of the anion was significantly larger than the ionic radius of the cation, the volume difference of the actuate membranes was generated, so that actuator exhibited cathodic deflection. When voltage was applied across the electrode, ion migration changed from the previous disordered state to ordered. The ion migration rate enhanced. Then, the ion concentration gradient was quickly established, which correspondingly reduced the resistance of the actuator membrane and enhanced the internal ion concentration and mechanical properties of the ion actuator sample.

2.2 Effect of NaCl on Electrochemical Performance of CSIA

The electrochemical performance of CSIA with different doping ratios was tested by cyclic voltammetry, and the cyclic voltammetry characteristic curves at different scanning speeds were shown in Fig.2(a-c), taking the specific capacitance at 50 $mV \cdot s^{-1}$ scanning speed as an example, with the increase of the doping rate of NaCl, the specific capacitance of the actuate membranes firstly increased to S_4 and then decreased to S_5. Specifically, the

specific capacitance of CS was up to 0.07719 $F \cdot g^{-1}$ in S_4, which was 1.58 times higher than that of 0.0299 $F \cdot g^{-1}$ of the capacitance of CSIA S_0. The specific capacitance value indicated the efficiency of ion migration in the sample to a certain extent, which might be due to the over crosslinking of the CSIA of the NaCl doped to interrupt the channel of ion migration in the actuate membranes, making its internal structure dense and uniform, thereby affecting the ion migration rate. In addition, the specific capacitance trend of the actuate membranes under different doping ratios and different scanning speeds were shown in Fig. 2(d-e). The specific capacitance of the actuate membranes gradually decreased as the scanning rate increased, which indicated that the scanning speed increase rate was faster than the area increases ratios of the CV curve. Finally, the relationship between the resistance of the actuate membrane and the specific capacitance was shown in Fig. 2(f). The two generally showed an inverse ratio, in the experimental group of S_4. The specific capacitance reached the maximum, the resistance reached the minimum, which corresponded to the output force of S_4, reflecting that the smaller the resistance, the larger the specific capacitance, the better the mechanical properties of the corresponding ion actuator.

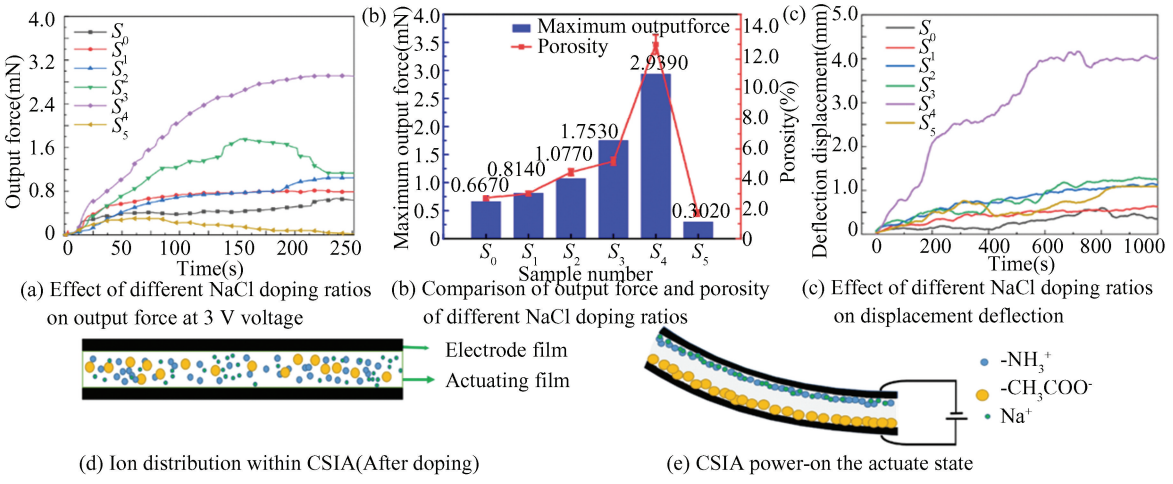

(a) Effect of different NaCl doping ratios on output force at 3 V voltage

(b) Comparison of output force and porosity of different NaCl doping ratios

(c) Effect of different NaCl doping ratios on displacement deflection

(d) Ion distribution within CSIA(After doping)

(e) CSIA power-on the actuate state

Fig.1 Mechonical properties and deflection mechanism

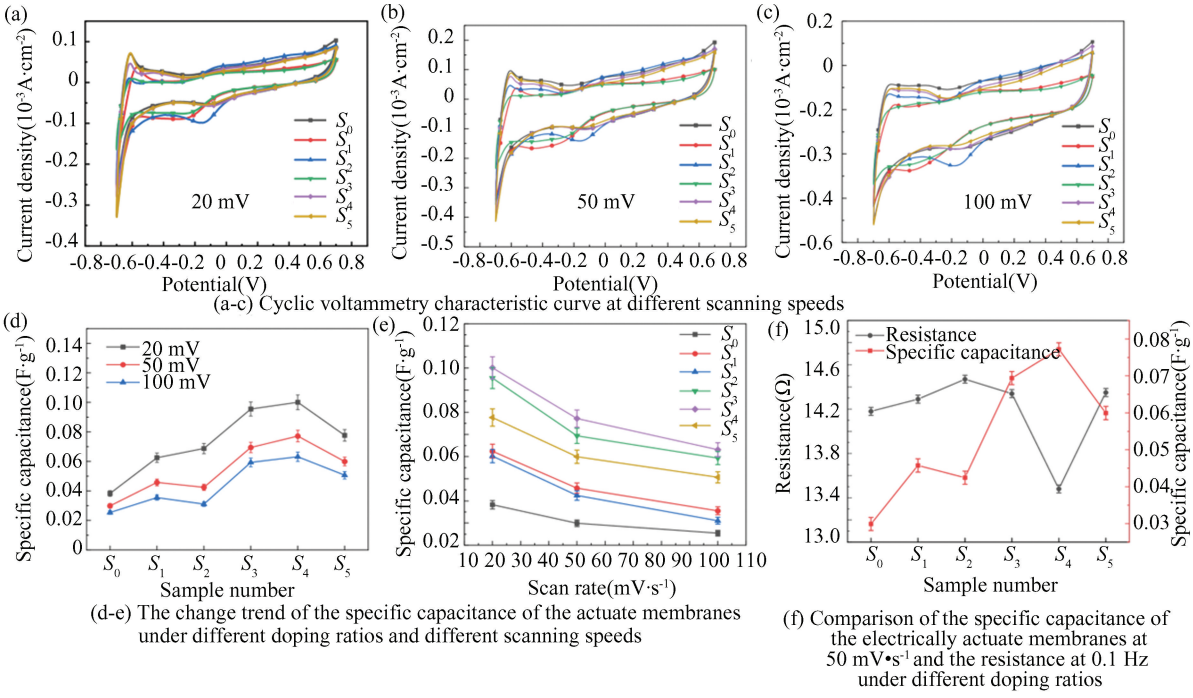

(a-c) Cyclic voltammetry characteristic curve at different scanning speeds

(d-e) The change trend of the specific capacitance of the actuate membranes under different doping ratios and different scanning speeds

(f) Comparison of the specific capacitance of the electrically actuate membranes at 50 mV•s^{-1} and the resistance at 0.1 Hz under different doping ratios

Fig. 2 Characteristic map of electrochemically relevant parameters

The relationship between the real resistance and virtual reactance of the CSIA actuate membranes were shown in Fig.3(a, b), and it could be seen that there was a good linear relationship between them. Curve fitting was performed by Z-view software and the equivalent circuit model is shown in Fig. S4(c). The line obtained by linear fitting intersects the x-axis, and the abscissa value of the intersection point was the resistance value of the actuate membrane of CSIA[31]. The resistance of the actuate membranes of CSIA were shown in Fig. 3(c). The resistance of the CSIA sample R_s could reflect the conductivity of the sample to a certain extent, taking 0.1 - 100000 Hz as an example, the resistance of the CSIA actuate membranes showed a trend of first decreasing and then increasing, in which the resistance of the actuate membrane at S_4 was 13.48 Ω, which was 4.937 % lower than that of the control group of S_0.

This showed that the CSIA sample achieved a better conductive effect at S_4 and appropriate NaCl cross-linking doping could improve the electrochemical performance of the CSIA, while excessive doping would intensify and change the molecular structure arrangement inside the actuate membrane of CSIA. This causes the ion channels to become clogged and crowded, increasing the resistance, and decreasing the electrochemical performance of CSIA.

As shown in Fig. 3(d), we can see the change in the conductivity of CSIA, and the best CSIA sample was more intuitive. When the measured conductivity changed from S_0 to S_5, the conductivity of CSIA showed a change curve, and the conductivity was maximum at S_4.

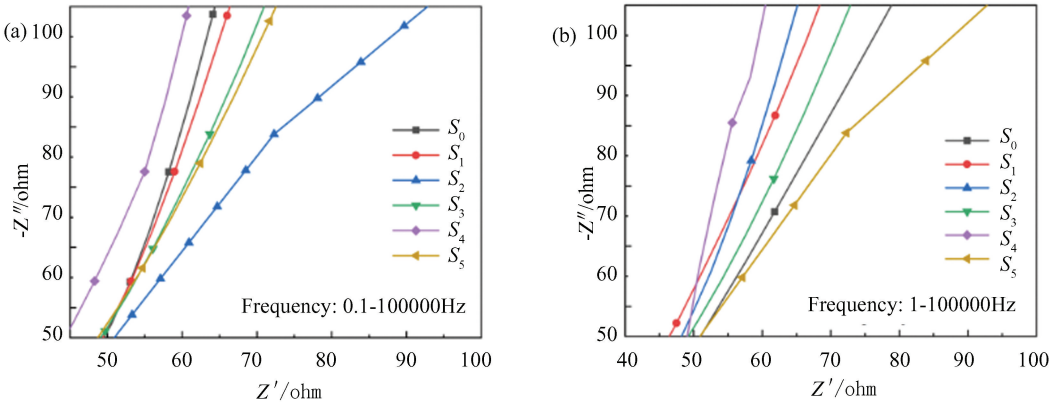

(a-b) Z-view fitted plot of different NaCl doping ratios at the low frequencies 0.1 Hz and 1 Hz

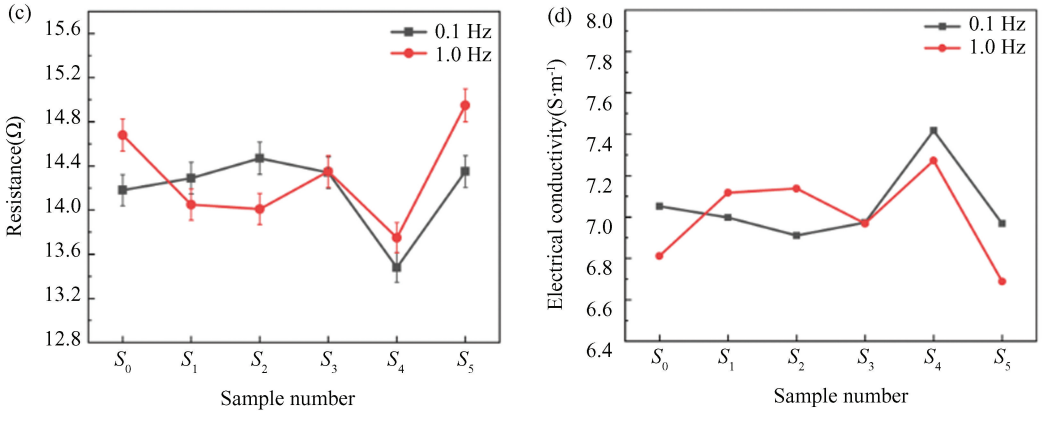

(c) Resistance of different NaCl doping ratios at the low frequencies 0.1 Hz and 1 Hz

(d) Electrical conductivity for different NaCl doping ratios at the low frequencies 0.1 Hz and 1 Hz

Fig.3

2.3 Effect of NaCl on Surface Morphology and Functional Groups of CSIA

2.3.1 *Electron microscopy scan of CSIA*

The micromorphology of the substrate surface and the side section under doped samples of CSIA S_0-S_5 were shown in Fig. 4. It could be seen from Fig.4(a-f) that the surface of the CSIA actuate membranes in the control group were smooth, and

with the increase of NaCl doping ratio, the particle size and roughness of the surface of the actuate membranes began to gradually increase. The particle size and roughness of CSIA increased significantly at S_5. In addition, the interface change between the electrode membranes and the actuate membranes of the CSIA doped with NaCl was shown in Fig.4(g-i).

Researchers had found that semi-interpenetrating network systems generally exhibit surprising properties that were superior to either of the two single polymers alone[32]. After observation and comparison, it was found that the undoped CSIA was smooth contact, while the interface of the NaCl-doped CSIA had an obvious three-dimensional physical cross-network structure. When a voltage was applied to the electrode, the ion migration changed from the previous disordered state to an ordered state. Ion mobility was improved. Then, the ion concentration gradient was rapidly established, which correspondingly reduced the resistance of the actuator membrane and increased the internal ion concentration and mechanical properties of the ion actuator sample.

This showed that the doping of NaCl had obvious changes to the internal structure of CSIA, which might be helpful to the performance of CSIA, but excessive doping would also be counterproductive.

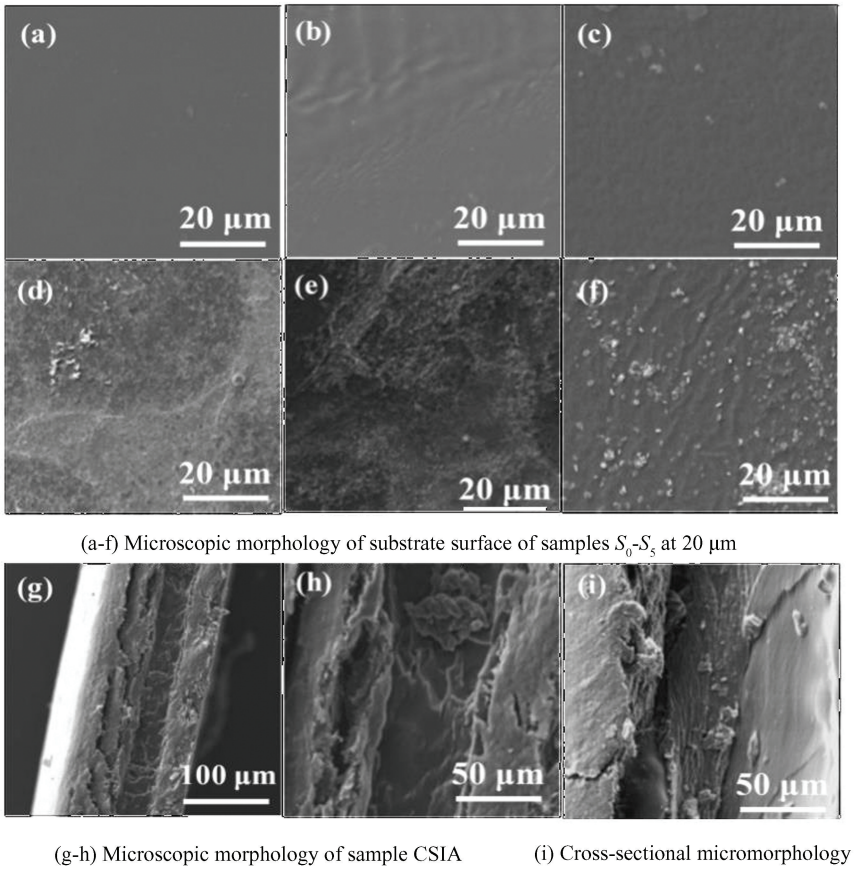

(a-f) Microscopic morphology of substrate surface of samples S_0-S_5 at 20 μm

(g-h) Microscopic morphology of sample CSIA at different sizes

(i) Cross-sectional micromorphology of CSIA samples without NaCl doped

Fig.4

2.3.2 Fourier transform infrared spectroscopy of CSIA

The FTIR spectra of CSIA sample S_0-S_5 was shown in Fig. 5. At 3376.79 cm^{-1} and 2929.28 cm^{-1}, they matched to the telescopic vibration peaks of −OH and $-NH_2$, respectively. The flexural vibration peaks was caused by $-CH_2$ and $-CH_3$ group near 1566.79 cm^{-1} and 1411.96 cm^{-1}. A tensile vibration peak was caused by $-CH_2-O-CH_2$ group narrowing 1045.12 cm^{-1} and bending vibration of $-CH_2-O-CH_2$ group neared 854. 10 cm^{-1}. From this group of functional groups, it could be preliminarily inferred that it was a functional group in the structure of CSIA, and the peaks of S_1-S_5 in the experimental group were basically the same as those in the control group, indicating that the CSIA of NaCl-doped had no significant effect on its functional groups.

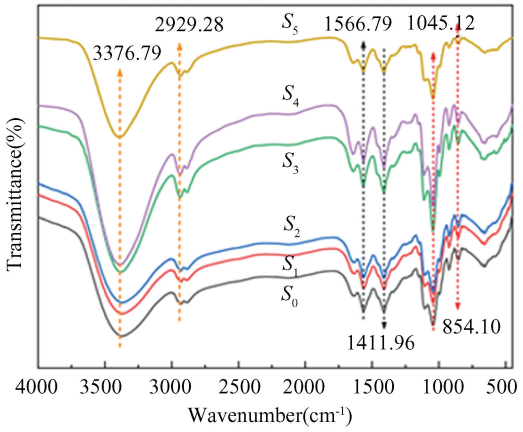

Fig. 5 FTIR spectra of CSIA samples of S_0–S_5 in the range of 4000–400 cm^{-1}

3 Conclusions

In order to explore the effect of sodium chloride on the enhanced performance of chitosan-based ion actuator (CSIA), sodium chloride doped CSIA were prepared by sol-gel method. Therefore, the effect of sodium chloride on CSIA were investigated. The mechanical properties of CSIA were tested by establishing an output force test platform while testing its porosity. The electrochemical performance was measured by electrochemical workstation. And the surface morphology and functional groups were measured by scanning electron microscopy and Infrared spectrogram, respectively. Then, the results indicated that the molar concentration of the sodium chloride was the best at 0.06836 mol·L^{-1} for CSIA. Its mechanical properties could reach an output force of 2.939 mN and a deflection displacement of 4.025 mm, and the maximum porosity of 12.98 % at the same time. The specific capacitance of the electrochemical performance was up to 0.07719 F·g^{-1}, and the minimum resistance reached 13.48 Ω. If the doping ratio of NaCl continued to increase, its output force, porosity and specific capacitance decreased to varying degrees. It turned out that over doping would block the internal three-dimensional structure of the CSIA, the ion channel would decrease, and the corresponding resistance would increase, resulting in a decrease in the output force performance. Through scanning electron microscopy, it showed that excessive doping of CSIA led to an increase in compactness and cracks between the surface and interface of membrane. The infrared showed that NaCl had no significant effect on the CSIA internal functional groups. The effective internal ion concentration and significantly reduced internal stress provided excellent performances under the appropriate voltage conditions. The doping of inorganic ion sodium chloride improved the internal electron transport efficiency of chitosan ion actuator, and advanced the mechanical properties of the actuator. This work was ultimately shown that the appropriate sodium chloride mass ratio had a great effect on the performance of CSIA. In future research work, the addition of glycerol to the experiment reduced the internal stress generated in the CSIA itself, and increasing the water content of CSIA enhanced the working life and storage conditions of the ion actuator.

Acknowledgment

The author wishes to acknowledge College of Material Science and Chemical Engineering, Harbin Engineering University for providing the required facilities. The authors would also like to thank Prof. Yanzhuo Lv, Dr. Yan Xu, Dr. Xiaoli Zhao, and Weikun Jia for providing the necessary facilities to conduct the experiments. The authors would also like to thank Prof. Yueming Ren for providing paper revisions. This work was supported by Key Laboratory of Engineering Bionics, Ministry of Education, Jilin University.

The authors commit that the design, data presentation, and citation of the study are in accordance with the standard COPE ethical guidelines and that appropriate approvals and consents have been obtained.

Supporting Information

Text S1. Preparation of Experimental Materials

Force measurement software (FA1004) was produced by Shanghai Shangping Instrument Co., Ltd (Shanghai, China). Vacuum drying oven (DZF-6050) was produced by Shanghai sead Instrument Co., Ltd (Shanghai, China). Electrochemical workstation (CHI760E) was produced by Shanghai Chenhua Instrument Co., Ltd. Infrared spectroscopy (FT-IR200) was produced by Tianjin Gangdong Technology Development Co., Ltd. Scanning electron microscope (S-240) was produced by Cambridge Instrument Company.

Chitosan (CS), sodium chloride (NaCl), acetic acid (HAC), Multi-walled carbon nanotubes (MCNT), Glycerol were provided by Shanghai Aladdin Bio-Chem Technology Co., Ltd (Shanghai, China). All chemicals were of analytic grade and used without treating further for purification and the deionized water was self-restraint.

In this experiment the ion actuator investigation was a new type of responsive electronic material, which was composed of electrode membranes and actuate membranes, in which the actuate membranes were mainly composed of multi-walled carbon nanotubes and chitosan, and the actuate membranes were composed of sodium chloride with different doping ratios and chitosan, acetic acid. Sodium chloride doped CSIA were prepared by sol-gel method[26].

Preparation of chitotan-based ion actuator as shown in Fig.S1. The CSIA preparation process consists of the following steps. First of all, 40 mL of acetic acid solution with a volume fraction of 2% was poured into six 250 mL beakers in a water bath at 50 ℃ to keep warm. Secondly, added 1.2 g chitosan to the beaker slowly and dissolved the solution thoroughly with magnetron stirring. Thirdly, different amounts of NaCl were added to different beakers in turn when the chitosan was completely dissolved. According to the experimental design, the doping ratios of NaCl added to the actuate membrane mixtures were detailed in Table S1. When mixtures completely dissolved, injected 2 mL of glycerol into the solution to obtain actuate membrane mixtures. Eventually, after ultrasonic defoaming for 15 min, the hydrogel was poured into a 50 mm×50 mm mold, placed in a drying oven, and dried at 50 ℃ for 12 h.

For the electrode film made of MCNT, take two pieces of CS base film solution as adhesive, apply them between the electrode film and the base film with a brush, form a sandwich structure, and physically press the parts under the condition of external pressure closure for about 10 h to make the MCNT electrode film and the CS base film bonded together.

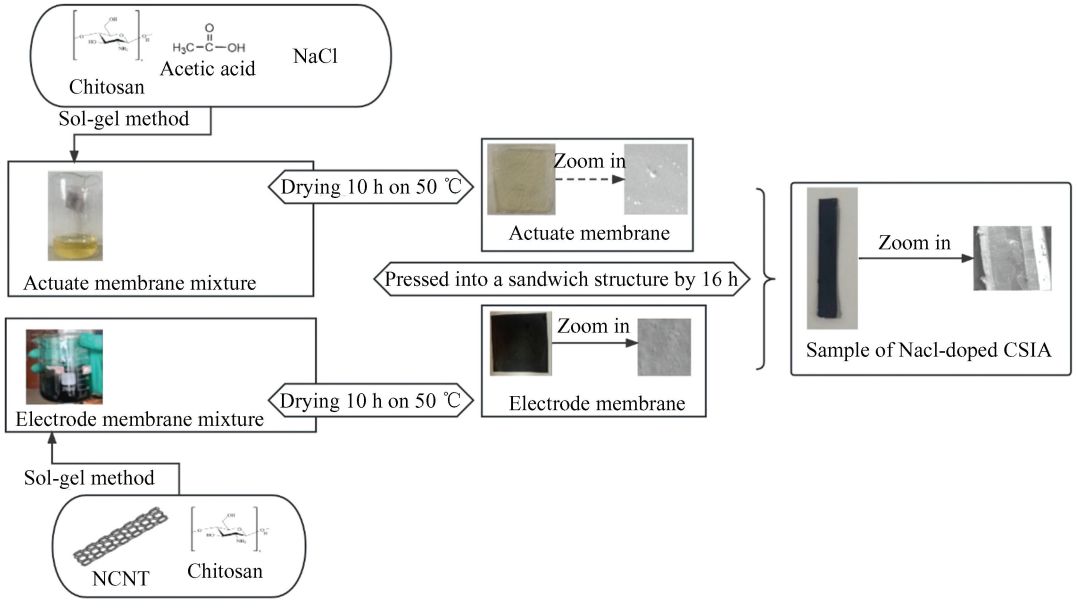

Fig. S1 Preparation of chitotan-based ion actuator

According to the experimental design, the doping ratio of NaCl added to the actuate membrane mixture was detailed in Table S1. Samples of CSIA of different NaCl qualities were numbered.

Notes:

The doping ratios of NaCl were the mass ratio of the chitosan solution of NaCl. For all groups, the chitosan ingredient was 1.2 g, glycerol was 2 mL and deionized water was 40 mL. The formula for calculating the molar concentration of NaCl proportion gel solution was shown below.

$$C = \frac{m}{M \times V} \quad (S1)$$

where C was the molar concentration of the NaCl ratio gel solution in mol · L^{-1}, m was the mass of NaCl doping, V was the gel solution volume of 40 mL and M was the molar fraction of NaCl with a value of 58.5 g · mol^{-1}.

Table S1 Ratio table of different CSIA raw materials

Sample	C (mol · L^{-1})
S_0	0
S_1	0.01709
S_2	0.03418
S_3	0.05127
S_4	0.06836
S_5	0.08545

The output force test platform was shown in Fig. S2(a). The output force test platform mainly included test software, DC power supply, gripping device, analyzing balance, etc. The test process was to provide a stable and controllable voltage to the actuator through the DC power supply, and the actuator under the support of the gripping device was measured by the analyzing balance in terms of the weight of the bending actuator, which was then analyzed and converted into the output force by the analyzing balance data transmission to the computer. The displacement test platform was shown in Fig. S2(b), which mainly includes test software, infrared sensor, grasping device, DC power supply, etc. The test process was to provide a stable and controllable voltage to the actuator through the DC power supply, which is gradually pressurized from 0 to 5 V, so that the actuator with the infrared sensor under the support of the grasping device and the data of the test was transmitted to the computer, and the amount of the deflected displacement was obtained through the data combing, and the maximal deflected displacement state could be measured after the end of the test.

When measuring the displacement, choose the infrared laser test point in the sample endpoint 3 mm. When the sample deflection, the farthest end would be offset to one side, but when the offset angle was too large will lead to the loss of the laser measurement point, resulting in the measurement can not continue. So choose to rely on the end point within a certain distance was better, after the actual measurement of the choice of 3 mm, this distance was better.

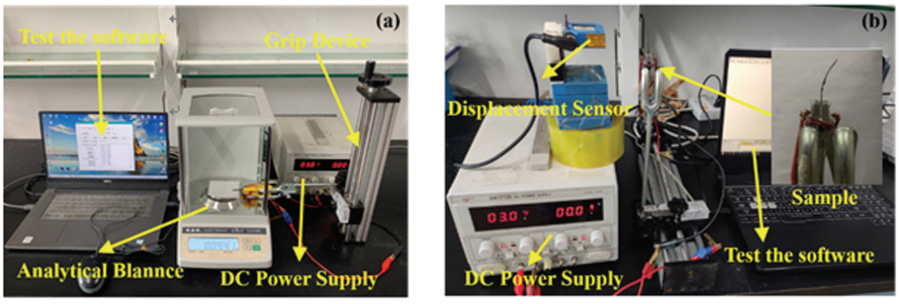

Fig.S2 (a) Output force test platform, and (b) Displacement test device platform

Text S2 Computational Details

The final deflection state diagram of the sample with different NaCl doping ratios at 5 V voltage was shown in Fig. S3, and the sample was removed after the displacement test and placed in a square with a scale value for comparative measurement, and the displacement amount identified in the figure was the vertical distance between the farthest end of the deflection end of the sample and the clamping end.

The electrochemical tests were tested by the electrochemical workstation, as shown in Fig. S4(a). The three-electrode system (Fig. S4(b)) was formed by using saturated calomel electrode as reference electrode and platinum electrode as auxiliary electrode and working electrode.

The equivalent circuit model was indicated in Fig.S4(c). It was used to study the electrochemical impedance data[29]. This analog circuit used R_s to represent the resistance of the electrolyte solution, R_{ct} to denote the charge transfer resistance, C_d to show the electric double-layer capacitance, and W_o to represent the open potential. Data fitting was performed using Z-view software. The reverse extension of the data in the figure was connected to the x-axis, and its intercept was the measured resistance value.

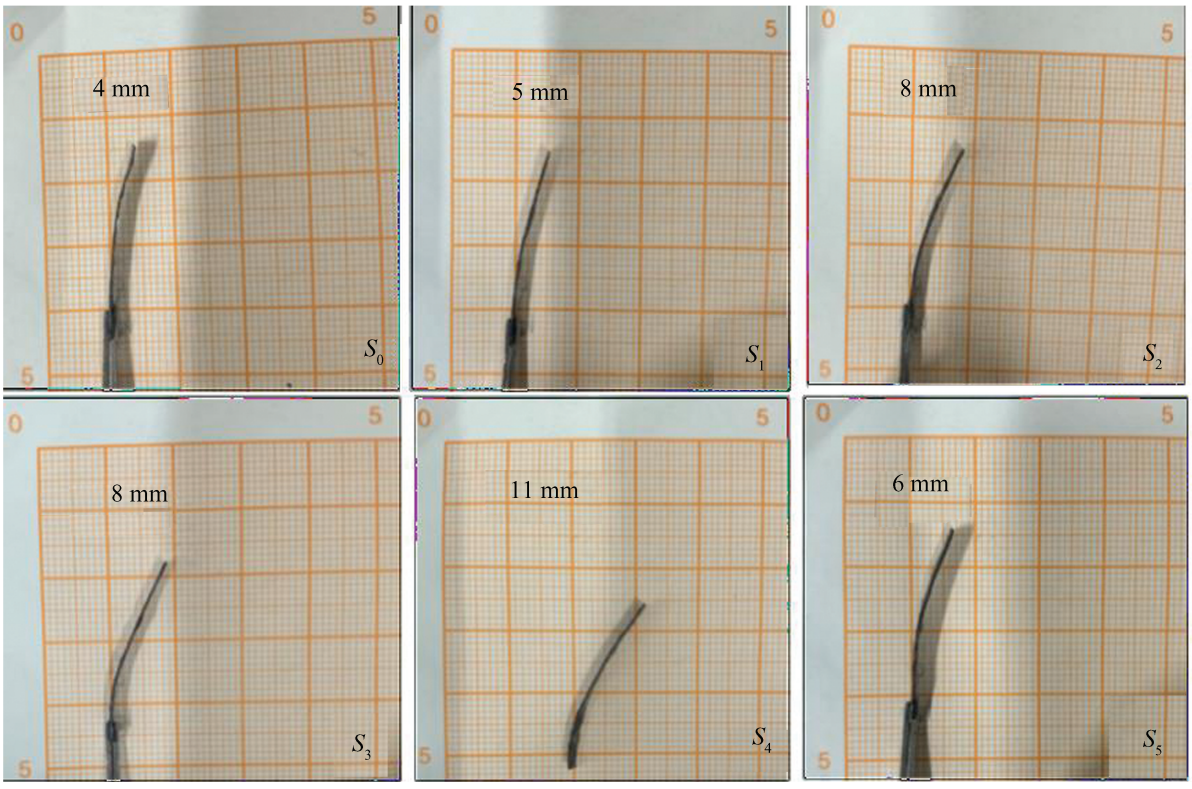

Fig. S3 Diagram of the final deflection state of samples with different NaCl doping ratios at 5 V voltage

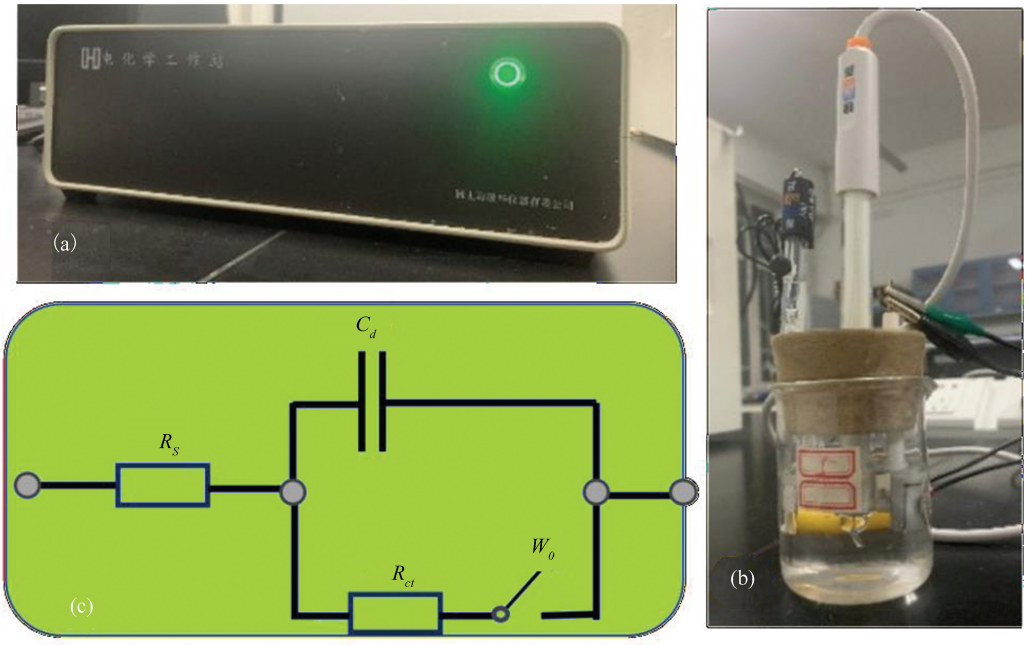

Fig. S4 (a) Electrochemical workstation; (b) three-electrode system; (c) Z-View analog circuitry

Table S2 Performance parameters of the sample

Sample number	Maximum output force(mN)	Maximum deflection displacement (mm)	Specific capacitance (50 mV·s^{-1}, F·g^{-1})	Resistance (0.1 Hz, Ω)	Porosity (%)
S_0	0.667	0.3524	0.02990	14.18	2.704
S_1	0.814	6.2790	0.04576	14.29	3.018
S_2	1.077	1.1270	0.04245	14.47	4.447
S_3	1.753	1.2430	0.06941	14.34	5.173
S_4	2.939	4.0250	0.07719	13.48	12.98
S_5	0.302	1.0890	0.05994	14.35	1.531

References

[1] Lasprilla A J, Martinez G A, Lunelli B H, et al. Polylactic acid synthesis for application in biomedical devices – a review. Biotechnology Advances, 2012, 30 (1): 321–328. DOI: 10.1016/j.biotechadv.2011.06.019.

[2] Gu G Y, Zhu J, Zhu L M, et al. A survey on dielectric elastomer actuators for soft robots. Bioinspir Biomim, 2017, 12(1): 011003. DOI: 10.1088/1748-3190/12/1/011003.

[3] Yuk H, Lin S, Ma C, et al. Hydraulic hydrogel actuators and robots optically and sonically camouflaged in water. Nature Communications, 2017, 8: 14230. DOI: 10.1038/ncomms14230.

[4] Henke E M, Schlatter S, Anderson I A. Soft dielectric elastomer oscillators driving bioinspired robots. Soft Robot, 2017, 4(4): 353–366. DOI: 10.1089/soro.2017.0022.

[5] Hirose M, Ogawa K. Honda humanoid robots development. Philos Trans A Math Phys Eng Sci, 2007, 365: 11–19. DOI: 10.1098/rsta.2006.1917.

[6] Kawaharazuka K, Nishiura M, Koga Y, et al. Automatic grouping of redundant sensors and actuators using functional and spatial connections: Application to muscle grouping for musculoskeletal humanoids. IEEE Robotics and Automation Letters, 2021, 6: 1981–1988. DOI: 10.1109/lra.2021.3060715.

[7] Kim S, Laschi C, Trimmer B. Soft robotics: a bioinspired evolution in robotics. Trends in Biotechnology, 2013, 31(5): 287–294. DOI: 10.1016/j.tibtech.2013.03.00.

[8] Tampieri A, Sandri M, Landi E, et al. HA/Alginate hybrid composites prepared through bio-inspired nucleation. Acta Biomater, 2005, 1(3): 343–351. DOI: 10.1016/j.actbio.2005.01.001.

[9] Wang Y, Fan C, Hu H, et al. Genetic modification of plant cell walls to enhance biomass yield and biofuel production in bioenergy crops. Biotechnology Advances, 2016, 34: 997–1017. DOI: 10.1016/j.biotechadv.2016.06.001.

[10] Marakana P G, Dey A, Saini B. Isolation of nanocellulose from lignocellulosic biomass: Synthesis, characterization, modification, and potential applications. Journal of Environmental Chemical Engineering, 2021, 9(6): 106606 DOI: 10.1016/j.jece.2021.106606.

[11] Dunlop M J, Acharya B, Bissessur R. Isolation of nanocrystalline cellulose from tunicates. Journal of Environmental Chemical Engineering, 2018, 6(4): 4408–4412. DOI: 10.1016/j.jece.2018.06.056.

[12] Wang H, Gurau G, Rogers R D. Ionic liquid processing of cellulose. Chemical Society Reviews, 2012, 41: 1519–1537. DOI: 10.1039/c2cs15311d.

[13] Caccavo D, Cascone S, Lamberti G, et al. Hydrogels: experimental characterization and mathematical modelling of their mechanical and diffusive behaviour. Chemical Society Reviews, 2018, 47: 2357–2373. DOI: 10.1039/c7cs00638a.

[14] Schmedlen R H, Masters K S, West J L. Photocrosslindable polyvinyl alcohol jydrogels that can be modified with cell adhision peptides for use in tissue engineering. Biomaterials, 2002, 23(22): 4325–4332. DOI: 10.1016/s0142-9612(02)00177-1.

[15] Zhai M L, Liu N, Li J, et al. Radiation preparation of PVA-g-NIPAAm in a homogeneous system and its application in controlled release. Radiation Physics and Chemistry, 2000, 57(3–6): 481–484. DOI: 10.1016/s0969-806x(99)00476-4.

[16] Peppas N A, Van Blarcom D S. Hydrogel-based biosensors and sensing devices for drug delivery. Journal of Controlled Release, 2016, 240: 142–150. DOI: 10.1016/j.jconrel.2015.11.02.

[17] Ohtaa M, Handaa A, Iwatab H, et al. Poly-vinyl alcohol hydrogel vascular models for in vitro aneurysm simulations the key to low friction surfaces. Technology and Health Care, 2004, 12(3): 225–233. DOI: 10.3233/thc-2004-12302.

[18] Yi Y, Xie C, Liu J, et al. Self-adhesive hydrogels for tissue engineering. Journal of Materials Chemistry B, 2021, 9: 8739–8767. DOI: 10.1039/d1tb01503f.

[19] Dolatabadi R, Mohammadi A, Walker R B. A novel three-dimensional printed device with conductive elements for electromembrane extraction combined with high-performance liquid chromatography and ultraviolet detector. Journal of Separation Science, 2022, 45: 3187–3196. DOI: 10.1002/jssc.202200028.

[20] Dolatabadi R, Zaheri M, Ebrahimi S, et al. A study on determination of theophylline in plasma and urine sample using electromembrane extraction combined with high-

performance liquid chromatography-ultraviolet. Chemical Papers, 2021, 76: 681-690. DOI:10.1007/s11696-021-01889-0.

[21] Amiri A, Mazaheri H. Study on the behavior of a temperature-sensitive hydrogel micro-channel via FSI and non-FSI approaches. Acta Mechanica, 2020, 231: 2799-2813. DOI:10.1007/s00707-020-02673-z.

[22] Niroumandi S, Shojaeifard M, Baghani M. PH-sensitive hydrogel-based valves: A transient fully-coupled fluid-solid interaction study. Journal of Intelligent Material Systems and Structures, 2021, 33: 196-209. DOI: 10.1177/1045389x211011671.

[23] Nourian A H, Amiri A, Moini N, et al. Synthesis, test, calibration and modeling of a temperature-actuated hydrogel bilayer. Smart Materials and Structures, 2020, 29. DOI:10.1088/1361-665X/ab9f46.

[24] Arbabi N, Baghani M, Abdolahi J, et al. Finite bending of bilayer pH-responsive hydrogels: A novel analytic method and finite element analysis. Composites Part B: Engineering, 2017, 110: 116-123. DOI: 10.1016/j.compositesb.2016.11.006.

[25] Ilyas R A, Sapuan S M, Bayraktar E. Bio and synthetic based polymer composite materials. Polymers (Basel), 2022, 14(18):3778. DOI:10.3390/polym14183778.

[26] Bokov D, Turki Jalil A, Chupradit S, et al. Nanomaterial by Sol-Gel method: synthesis and application. Advances in Materials Science and Engineering, 2021, 2021: 1-21. DOI: 10.1155/2021/5102014.

[27] Antonietti M, Fechler N, Fellinger T P. Carbon aerogels and monoliths: control of porosity and nanoarchitecture via Sol-Gel routes. Chemistry of Materials, 2014, 26: 196-210. DOI: 10.1021/cm402239e.

[28] Zhang M, Yang D Y, Li J T. Supercapacitor performances of MnO2 and MnO2/ reduced graphene oxide prepared with various electrodeposition time. Vacuum, 2020, 178: 109455. DOI: 10.1016/j.vacuum.2020.109455

[29] Panwar V, Ko SY, Park J-O, et al. Enhanced and fast actuation of fullerenol/PVDF/PVP/PSSA based ionic polymer metal composite actuators. Sensors and Actuators B: Chemical, 2013, 183: 504-517. DOI: 10.1016/j.snb.2013.04.037.

[30] Kim J., Wang N, Chen Y. Effect of chitosan and ions on actuation behavior of cellulose-chitosan laminated films as electro-active paper actuators. Cellulose, 2007, 14: 439-445. DOI: 10.1007/s10570-007-9134-z.

[31] Sun Z, Yang L, Zhang D. High performance, flexible and renewable nano-biocomposite artificial muscle based on mesoporous cellulose/ ionic liquid electrolyte membrane. Sensors and Actuators B: Chemical, 2019, 283: 579-589. DOI: 10.1016/j.snb.2018.12.073.

[32] Myung D, Waters D, Wiseman M. Progress in the development of interpenetrating polymer network hydrogels. Polymers for Advanced Technologies, 2008, 19: 647-657. DOI: 10.1002/pat.1134.